International Journal of Heat and Mass Transfer 94 (2016) 87–100

Contents lists available at ScienceDirect

International Journal of Heat and Mass Transfer

journal homepage: www.elsevier.com/locate/ijhmt

Double MRT thermal lattice Boltzmann simulation for MHD natural convection of nanofluids in an inclined cavity with four square heat sources

Tao Zhang, Defu Che *

State Key Laboratory of Multiphase Flow in Power Engineering, School of Energy and Power Engineering, Xi'an Jiaotong University, Xi'an, Shaanxi 710049, PR China

ARTICLE INFO

Article history:
Received 25 May 2015
Accepted 19 November 2015
Available online 1 December 2015

Keywords:
Lattice Boltzmann method
Double multiple-relaxation-time
Magneto-hydrodynamic
Nanofluids
Natural convection
Inclined square cavity

ABSTRACT

In this paper, a two-dimensional double multiple-relaxation-time (MRT) thermal lattice Boltzmann model was developed to simulate the magneto-hydrodynamic (MHD) flow and heat transfer of Cu–water nanofluids in an inclined cavity with four heat sources. For the outer square cavity, the top and down walls were thermally insulated and the other two walls were maintained at a constant temperature. While for the four square heat sources, the outer walls were kept at a higher constant temperature. The space between the outer square and the inner heat source was filled with a nanofluid composed of the water and the Cu spherical nanoparticles. The flow and temperature fields were solved with the D2Q9-MRT and D2Q5-MRT model, which have been validated by previous investigations. Based on the double MRT thermal lattice Boltzmann model, the effects of the Hartmann number, the Rayleigh number, the inclination angle, and the volume fraction of nanoparticles on the fluid flow and heat transfer are investigated in the study. The results show that the addition of Cu shows greater impact on the flow fields than on the temperature patterns. The inclination angle and the Hartmann number present a significant influence on the flow and temperature patterns. The average Nusselt number increases significantly with the increase of nanoparticles volume fraction, but it decreases in the presence of a magnetic field at any given Rayleigh number and inclination angle. In addition, for high Rayleigh numbers, the average Nusselt number decreases at first as the inclination angle increases to a specific inclination angle and then increases with further increased inclination angle at low Hartmann numbers, while at high Hartmann numbers, The average Nusselt number increases at first as the inclination angle increases to a certain inclination angle and then decreases with further increased inclination angle. The results are expected to provide supplementary data and also a validation of LBM for simulations in engineering applications.

1. Introduction

The classical problem of natural convection flow and heat transfer in enclosures has many engineering and environmental applications such as heat exchangers, nuclear and chemical reactors, cooling of electronic systems, energy systems, space technologies (creation of reliable cooling system for airborne electronics, heat pipes) and furnace engineering [1–4]. In most of the previous studies [5–7] on natural convection in enclosures, the base fluids in common use, such as water, ethylene glycol and engine oil, often have low thermal conductivity, which in turn limits the enhancement of the heat transfer. To overcome this drawback, there is a strong motivation to develop advanced heat transfer fluids with substantially higher conductivities to enhance thermal characteristics. Nanofluids, a suspension of nanoparticles into conventional fluids, have been considered as an effective medium in views of its abnormally higher thermal conductivity [8]. Compared with micron-sized particles, nano-phase has much larger relative surface areas and a great potential for heat transfer enhancement. At this circumstance, the use of nanofluids can be considered as a promising solution [9–13].

The study of natural convection heat transfer within systems using nanofluids has been carried out in differentially heated enclosures. Khanafer et al. [14] numerically investigated the natural convection heat transfer of a copper–water nanofluid in a differentially heated square cavity. They found that the heat transfer rate increases with an increase in the nanoparticle volume fraction at any given Rayleigh number in their study. Ho et al. [15] numerically examined the effect of uncertainties due to adopting different formulas for the effective thermal conductivity and dynamic viscosity. They simulated natural convection heat transfer

* Corresponding author. Tel.: +86 29 8266 5185; fax: +86 29 8266 8703.
E-mail address: dfche@mail.xjtu.edu.cn (D. Che).

http://dx.doi.org/10.1016/j.ijheatmasstransfer.2015.11.071
0017-9310/

Nomenclature

B	magnetic field strength
c	lattice speed
$\boldsymbol{e}_i$	discrete lattice velocity in direction
f_i	distribution function for flow
g_i	distribution function for temperature
$\boldsymbol{F}_i$	external force
$\boldsymbol{g}$	gravitational acceleration
Gr	Grash number
H	length of the square cavity
Ha	Hartmann number
Ma	Mach number
Nu	Nusselt number
P	pressure
Pr	Prandtl number
Ra	Rayleigh number
T	temperature, K
$\boldsymbol{u}$	velocity
w_i	weight coefficient in direction i
$\boldsymbol{x}$	space coordinate in a 2D lattice
$\boldsymbol{x}_b$	the boundary node
$\boldsymbol{x}_f$	the nearest neighbor fluid node of x_b
x	coordinates defined in Fig. 1

Greek letters

α	thermal diffusivity
β	volume expansion coefficient
δ_t	lattice time step
δ_x	grid step
φ	solid volume fraction
k	thermal conductivity
λ	inclination angle
ν	kinematic viscosity
ρ	density
τ_v	relaxation time for flow
τ_T	relaxation time for temperature

Subscripts

0	initial, or ambient
c	cold wall
f	base fluid
h	hot wall
m	average
i	direction of micro velocity
nf	nanofluid
p	nanoparticle

Superscripts

eq	equilibrium
neq	nonequilibrium

in a vertical square enclosure filled with an Al_2O_3–water nanofluid and found that the heat transfer across the enclosure could be enhanced or mitigated depending on the formulas used for the estimated dynamic viscosity of the nanofluids. Nnanna [16] experimentally examined the heat transfer behavior of a buoyancy-driven Al_2O_3–water nanofluid in a two dimensional rectangular cavity with differentially heated vertical walls and adiabatic horizontal walls. He developed an empirical correlation for Nusselt number as a function of the volume fraction of the nanoparticles and the Rayleigh number and argued that the enhanced heat transfer rate can be achieved at a small volume fraction of nanoparticles. Ghasemi and Aminossadati [17] numerically investigated the influences of pertinent parameters such as Rayleigh numbers, inclination angles and solid volume fractions on the heat transfer characteristics of natural convection in a square cavity. The results showed that adding nanoparticles into the pure water improves its heat transfer performance; however, there is an optimum solid volume fraction which maximizes the heat transfer rate. Abu-Nada and Oztop [18] studied the buoyancy-induced flow in a wavy walled cavity. They found that the geometry parameter is more effective on the flow fields than that of temperature distributions. Akhtari et al. [19] presented an experimental and numerical study on the heat transfer of nanofluids flowing in the heat exchangers under laminar flow conditions. The results indicated that the heat transfer performance of the heat exchangers increases with increasing the hot and cold volume flow rates, as well as the particle concentrations and nanofluids inlet temperature. Most of the previous studies on natural convection in enclosures have focused on either vertical or horizontal heat sources. However, in a variety of applications, enclosures are inclined with respect to the acceleration of gravity, so that the buoyancy force has both tangential and normal components relative to the differentially heated walls. In these cases, the flow structure and heat transfer through the cavity are affected by the inclination angle. Sourtiji et al. [20] studied the unsteady periodic natural convection flows through an alumina-water nanofluid in a square cavity due to a sinusoidal time-dependent temperature of a thin heat source located at the center of the enclosure. They found that the performance of the nanoparticle utilization on the enhancement of the heat transfer at higher Rayleigh numbers is less than that of lower Rayleigh numbers. Pourmehran et al. [21] applied collocation method, least square method and fourth-order Runge–Kutta method to unsteady flow of a nanofluid squeezing between two parallel plates. The results of least square method are more accurate than collocation method. Later, they presented a thermal and flow analysis of a fin shaped

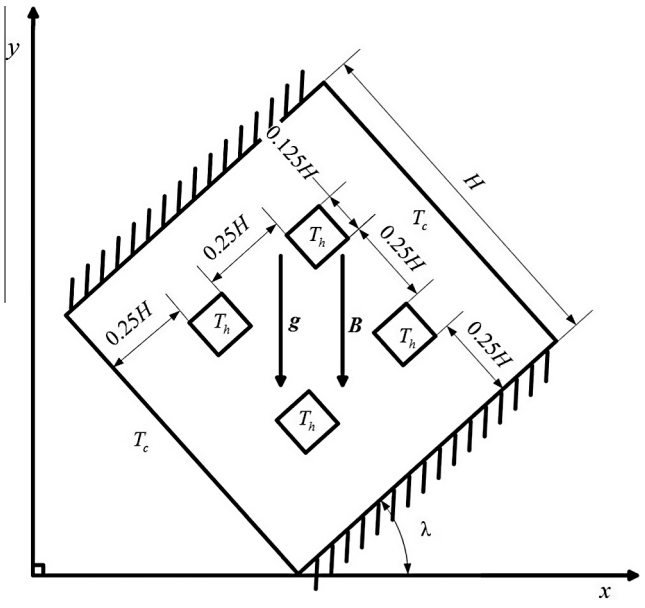

Fig. 1. Schematic diagram of the physical model and coordinate system.

microchannel heat sink cooled by different nanofluids and found that Nusselt number enhancement has direct relationship with inertial force parameter and volume flow rate [22]. An analytical investigation was applied to unsteady motion of a rigid spherical particle in a quiescent shear-thinning power-law fluid by Rahimi-Gorji et al. [23]. The results showed that collocation method is simpler and more accurate than other method. Recently, Rahimi-Gorji et al. [24] numerically studied the effect of different nanofluids on the heat transfer for the microchannel heat sink. The results showed that the Brownian movement of the particles increases by increasing the nanoparticles volume fraction and consequently the difference between coolant and wall temperature becomes less.

The effect of the magnetic field on the heat transfer and fluid flow has received considerable attention during the recent years due to its importance in some practical cases such as the crystal growth in fluids, the metal casting, the fusion reactors and the geothermal energy extractions. The existence of a magnetic field has a noticeable effect on heat transfer reduction under natural convection. Several studies have been conducted to evaluate the effect of the magnetic field on natural convection flow and heat transfer in cavities filled with electrically conducting fluids. Rashidi et al. [25] studied the effects of heterogeneous heating on natural convection of Al_2O_3–water nanofluid in a square cavity. They found that the Nusselt number is minimized where the heat flux in the vicinity of adiabatic wall is smallest while the heat flux near the cold wall is biggest for high values of Rayleigh number.

Sathiyamoorthy and Chamkha [26] examined the steady laminar tow-dimensional natural convection in the presence of an inclined magnetic field in a square enclosure filled with a liquid gallium. They found that the heat transfer decreases with an increase in the magnetic intensity and the vertically and horizontally applied magnetic fields affect the heat transfer differently. Magnetic field effect on entropy generation in a nanofluid-filled enclosure with sinusoidal heating on both side walls was presented by Mejri et al. [27]. The results showed that the heat transfer rate and entropy generation respectively increase and decrease with the increases of volume fraction and the proper choice of Rayleigh number, Hartmann number, phase deviation, and solid volume fraction could be able to maximize heat transfer rate simultaneously minimizing entropy generation. A numerical study of natural convection in a square cavity with a thin fin that is under the influence of a uniform magnetic field was presented by Aminossadati et al. [28]. The results showed that the flow and temperature fields and the heat transfer rate of the cavity are all influenced by the magnetic field, especially at higher Rayleigh number. As the Hartmann number increases, the magnetic field limits the convective flow circulations and, as a result, the heat transfer rate decreases. Bourantas and Loukopoulos [29] developed a mesh-less point collocation method utilizing a velocity correction scheme to investigate the MHD natural convection flow in the presence of a magnetic field in an inclined rectangular enclosure. The results showed that both the strength and orientation of the magnetic field significantly affect the flow and temperature fields. Selimefendigil and Oztop [30] performed a numerical study of MHD mixed convection lid driven square enclosure filled with nanofluids. They found that averaged heat transfer decreases with increasing the Hartmann number while increases as the solid volume fraction increases.

The LBM has been demonstrated to be a very effective numerical tool and various models have been built to investigate the thermal fields and hydrodynamics that are problematic for conventional methods [31–36]. The LBM was developed to investigate the nanoparticles distribution and flow pattern of nanofluids by Xuan and Yao [37]. They found that the flow and rising temperature of the fluid can improve the nanoparticles distribution, which is beneficial to energy transport enhancement of nanofluids. Nemati et al. [38] studied the natural convection heat transfer in an lid-driven cavity by lattice Boltzmann Method. The results indicated that the effect of solid volume fraction grows stronger sequentially for fluids containing Al_2O_3, CuO, and Cu nanoparticles. In addition, the increase of the Reynolds number leads to a decrease of the solid concentration effect. Recently, LBM simulation of turbulent natural convection with large-eddy simulations (LES) in a square cavity filled with water/copper nanofluids was investigated by Sajjdai et al. [39]. The results indicated that heat transfer declines with the increase in the aspect ratios, but the effect of nanoparticles is dissimilar for various aspect ratios at different Rayleigh numbers. Kefayati [40] applied lattice Boltzmann method to simulate the heat dissipation effect of a ferrofluid on natural convection flow in the presence of an external magnetic source. Zhang and Che [41] studied the natural convection heat transfer in an inclined square cavity using the lattice Boltzmann method. They found that the inclination angle and the heat source length have a significant impact on the flow and temperature fields and the heat transfer rate. Kefayati [42] analyzed the effect of a magnetic field on natural convection flow in a nanofluid-filled cavity with sinusoidal temperature distribution by lattice Boltzmann method. The results showed that the heat transfer is decreased by the increment of Hartmann number for various Rayleigh numbers. Also the magnetic field augments the effect of nanoparticles at high Rayleigh numbers. Sheikholeslami and Gorji [43] studied the free convection of ferrofluid in a cavity heated from below in the presence of an external magnetic field. The results showed that particles with a smaller size have better ability to dissipate heat, and a larger volume fraction would provide a stronger driving force which leads to increase in temperature profile. Sheikholeslami et al. [44] studied the magneto-hydrodynamic natural convection heat transfer of Al_2O_3-Water nanofluid in a horizontal cylindrical enclosure with an inner triangular cylinder. They found that the value of the maximum stream function decreases with increasing Hartmann number. Elshehabey and Ahmed [45] presented a numerical investigation on MHD mixed convection in a lid-driven cavity filled with nanofluid. The results showed that the presence of an inclined magnetic field in the flow region leads to lose the fluid movement.

Despite a number of studies on MHD natural convection heat transfer using nanofluids reported in the previous literature, there is still a serious lack of information regarding the problem of MHD heat transfer of nanofluids in inclined enclosures with complicated geometric objects. Therefore, more works will be required in order to better understand the fluid dynamic and thermal characteristics of nanofluids in the presence of a magnetic field. In fact, to the best knowledge of the authors, no studies have been reported before in the literature to investigate the MHD natural convection of nanofluids in inclined square enclosures with four heat sources using double multiple-relaxation-time (MRT) thermal lattice Boltzmann method, which has superior numerical features compared to that of the single relaxation time. Thus, the main objective of the present work is to establish a double multiple-relaxation-time (MRT) thermal lattice Boltzmann method as a viable tool for the simulation of magneto-hydrodynamic (MHD) flow and heat transfer of Cu–water nanofluids in an inclined square enclosure with four inner square heat sources. In this model, the flow and temperature fields are solved with the D2Q9-MRT model and the D2Q5-MRT model, respectively, and the results of this solution are validated with previous numerical investigations. The effects of the Hartmann number, the Rayleigh number, the inclination angle, and the volume fraction of nanoparticles on the fluid flow and heat transfer process are studied and the results are expected to provide supplementary data and also a validation of LBM for simulations in engineering applications.

2. Problem description

The schematic of the physical model is shown in Fig. 1. The edge length of the outer square cavity is H. There are four square heat sources in the square cavity and the side length of all square heat sources in the square is 0.125 H. The distance between the side of the outer square cavity and the outer side of each square heat source is 0.25 H. The gap between each square heat source is also 0.25 H. For the outer square cavity, the top and down walls are thermal insulated and the other two walls are maintained at a constant temperature, T_c. While a constant temperature, T_h, is applied on each out wall of the four square heat sources. The space between the outer square and the inner heat sources is filled with a nanofluid composed of the water and the Cu spherical nanoparticles. The nanofluid is assumed to be Newtonian and incompressible. The base fluid (water) and the spherical nanoparticles (Cu) are presumed to be in thermal equilibrium. The inclination angle, λ, ranges from 0° to 90° in this simulation. For $\lambda = 0^{\circ}$, the two cold walls are parallel with the acceleration of gravity, $\boldsymbol{g}$. The magnetic field of strength B is applied in the same direction as the gravity. All walls are impermeable. The flow is considered to be steady and laminar. The length of the inner and outer enclosure perpendicular to the figure is large enough to reduce the present problem to a two-dimensional one.

3. Numerical procedure

3.1. D2Q9-MRT-LBE model for the flow problem

For the flow fields, the continuous Boltzmann equation is written as follows:

$$\frac{\partial f_i}{\partial t} + \boldsymbol{e}_i \cdot \nabla f_i = \Omega_i(f) = -\frac{1}{\tau}\left[f_i(\boldsymbol{r}_j, t) - f_i^{eq}(\boldsymbol{r}_j, t)\right] \tag{1}$$

where $f_i(\boldsymbol{r}_j, t)$ is the volume-averaged discrete distribution function with D2Q9 velocity $\boldsymbol{e}_\alpha$ at lattice node r_j, $\Omega_i(f)$ is the discrete collision operator, f_i^{eq} is the discrete equilibrium distribution function, and, τ is the dimensionless relaxation time. After introducing BGK approximation, the commonly used discretized form of Eq. (1), which employs a single relaxation time (SRT) model to simulate the evolution of macroscopic quantities (such as density, pressure and velocity), can be written as:

$$f_i(\boldsymbol{r}_j + \boldsymbol{e}_i\delta_t, t + \delta_t) - f_i(\boldsymbol{r}_j, t) = \Omega_i(f) = -\frac{1}{\tau}[f_i(\boldsymbol{r}_j, t) - f_i^{eq}(\boldsymbol{r}_j, t)] \tag{2}$$

In order to improve the numerical stability and accuracy of the lattice Boltzmann method, the MRT collision operator [46] was proposed as follows:

$$\Omega_i(f) = -\boldsymbol{\Lambda}[f_i(\boldsymbol{r}_j, t) - f_i^{eq}(\boldsymbol{r}_j, t)] \tag{3}$$

where $\boldsymbol{\Lambda} = \boldsymbol{M}^{-1}\boldsymbol{S}\boldsymbol{M}$ is the collision matrix, $\boldsymbol{M}$ is an orthogonal transformation matrix, $\boldsymbol{S}$ is a diagonal matrix. The relaxation times for hydrodynamic and non-hydrodynamic moments can be separated. The MRT-LBM evolution equations [47] with forcing term C_i can be written as:

$$f_i(\boldsymbol{r}_j + \boldsymbol{e}_i\delta_t, t + \delta_t) - f_i(\boldsymbol{r}_j, t) = -\boldsymbol{\Lambda}[f_i(\boldsymbol{r}_j, t) - f_i^{eq}(\boldsymbol{r}_j, t)] + C_i \tag{4}$$

The D2Q9 model with standard two dimensional, nine velocities square lattice for flow part is used in this work. The discrete velocities in the D2Q9 model take the form [48]:

$$\boldsymbol{e}_i = \begin{cases} (0,0), & i = 0 \\ c\left(\cos\left[(i-1)\frac{\pi}{2}\right], \sin\left[(i-1)\frac{\pi}{2}\right]\right), & i = 1,2,3,4 \\ \sqrt{2}c\left(\cos\left[(2i-1)\frac{\pi}{4}\right], \sin\left[(2i-1)\frac{\pi}{4}\right]\right), & i = 5,6,7,8 \end{cases} \tag{5}$$

where, $c = \delta_x/\delta_t$ is the lattice speed, in which δ_x is the grid step and δ_t is the time step. Based on this lattice model, the density distribution function $f_i(\boldsymbol{r}_j, t)$ can be projected onto the moment space with $\boldsymbol{m} = \boldsymbol{M}\boldsymbol{f} = (\rho, e, \varepsilon, j_x, q_x, j_y, q_y, p_{xx}, p_{xy})^{\mathrm{T}}$ through the transformation matrix. And in this order, these nine moments have the following physical meaning: ρ is the fluid density, e is the energy mode, ε is related to energy square, (j_x, j_y) are the momentum components, (q_x, q_y) correspond to the energy flux, and (p_{xx}, p_{xy}) are related to the diagonal and off-diagonal components of the stress tensors, respectively. With the ordering of the above specified velocity moments, the corresponding transform matrix $\boldsymbol{M}$ is given by [46]:

$$\boldsymbol{M} = \begin{bmatrix} 1 & 1 & 1 & 1 & 1 & 1 & 1 & 1 & 1 \\ -4 & -1 & -1 & -1 & -1 & 2 & 2 & 2 & 2 \\ 4 & -2 & -2 & -2 & -2 & 1 & 1 & 1 & 1 \\ 0 & 1 & 0 & -1 & 0 & 1 & -1 & -1 & 1 \\ 0 & -2 & 0 & 2 & 0 & 1 & -1 & -1 & 1 \\ 0 & 0 & 1 & 0 & -1 & 1 & 1 & -1 & -1 \\ 0 & 0 & -2 & 0 & 2 & 1 & 1 & -1 & -1 \\ 0 & 1 & -1 & 1 & -1 & 0 & 0 & 0 & 0 \\ 0 & 0 & 0 & 0 & 0 & 1 & -1 & 1 & -1 \end{bmatrix} \tag{6}$$

Among the nine velocity moments, only the density $m_0 = \rho$ and the momentum $m_{3,5} = j_{x,y}$ are conserved quantities, while the other six velocity moments are non-conserved quantities.

The local equilibrium density distribution functions can be given by [36]:

$$f_i^{eq} = \begin{cases} \rho_0 - \frac{5p}{3c^2} + \rho_0 s_i(\boldsymbol{u}) & i = 0 \\ \frac{p}{3c^2} + \rho_0 s_i(\boldsymbol{u}) & i = 1,2,3,4 \\ \frac{p}{12c^2} + \rho_0 s_i(\boldsymbol{u}) & i = 5,6,7,8 \end{cases} \tag{7}$$

$$s_i(\boldsymbol{u}) = w_i\left(1 + 3\frac{\boldsymbol{e}_i \cdot \boldsymbol{u}}{c^2} + 4.5\frac{(\boldsymbol{e}_i \cdot \boldsymbol{u})^2}{c^2} - 1.5\frac{u^2}{c^2}\right) \tag{8}$$

The lattice weights w_i are given as follows: $w_0 = 4/9$, $w_i = 1/9$ for $i = 1,2,3,4$ and $w_i = 1/36$ for $i = 5,6,7,8$. Based on the equilibrium distribution function f_i^{eq}, $f_i^{eq}(\boldsymbol{r}_j, t)$ can be projected onto the moment space with $\boldsymbol{m}^{eq} = \boldsymbol{M}\boldsymbol{f}^{eq} = (\rho_0, e^{eq}, \varepsilon^{eq}, j_x, q_x^{eq}, j_y, q_y^{eq}, p_{xx}^{eq}, p_{xy}^{eq})^{\mathrm{T}}$. The equilibrium moments $\boldsymbol{m}^{eq}$ of the present model can be constructed accordingly as [49]:

$$\begin{aligned} m_1^{eq} &= e^{eq} = -4 + 6p + 3\rho_0|\boldsymbol{u}|^2 \\ m_2^{eq} &= \varepsilon^{eq} = 4 + 9p + 3\rho_0|\boldsymbol{u}|^2 \\ m_4^{eq} &= q_x^{eq} = \rho_0 u_x \\ m_6^{eq} &= q_y^{eq} = \rho_0 u_y \\ m_7^{eq} &= p_{xx}^{eq} = \rho_0(u_x^2 - u_y^2) \\ m_8^{eq} &= p_{xy}^{eq} = \rho_0 u_x u_y \end{aligned} \tag{9}$$

In this simulation, the mean fluid density ρ_0 is set to be 1 for simplicity. The incompressibility approximation, i.e., $(j_x, j_y) \approx \rho_0\boldsymbol{u}$, has been use in the equilibrium moments.

As suggested by Lallemand and luo [49], the non-conserved moments relax linearly towards their equilibrium values. Therefore, for the D2Q9 model, the collision process of the MRT method is accomplished as follows:

$$\boldsymbol{m}^{+} = \boldsymbol{m} - \boldsymbol{\Lambda}(\boldsymbol{m} - \boldsymbol{m}^0) + \delta_t\left(\boldsymbol{I} - \frac{\boldsymbol{\Lambda}}{2}\right)\boldsymbol{C} \tag{10}$$

where $\boldsymbol{I}$ is the 9×9 unit matrix. The streaming step is still carried out in the velocity space by:

$$f_i(\boldsymbol{r}_j + \boldsymbol{e}_i\delta_t, t + \delta_t) = f_i^{+}(\boldsymbol{r}_j, t) \tag{11}$$

where $\boldsymbol{f}^{+}=\boldsymbol{M}^{-1}\boldsymbol{m}^{+}$.

In the present work, the total body force $\boldsymbol{F}$ is included by adding a forcing term to the collision step in the moment space with the fluid velocity being redefined. $\boldsymbol{F}$ can be defined as $\boldsymbol{F}_i=w_i[(\boldsymbol{e}_i\cdot\boldsymbol{a})/(RT_0)+\boldsymbol{u}\boldsymbol{a}:(\boldsymbol{e}_i\boldsymbol{e}_i-RT_0\mathbf{I})/(RT_0)^2]$ [50]. The components of the forcing term $\boldsymbol{C}$ in the moment space are given by:

$$\begin{aligned}&C_0=0,\quad C_1=6\rho_0\boldsymbol{u}\cdot\boldsymbol{a},\quad C_2=-6\rho_0\boldsymbol{u}\cdot\boldsymbol{a}\\&C_3=\rho_0a_x,\quad C_4=-\rho_0a_x,\quad C_5=\rho_0a_y\\&C_6=-\rho_0a_y,\quad C_7=2\rho_0(u_xa_x-u_ya_y),\quad C_8=\rho_0(u_xa_y+u_ya_x)\end{aligned}\tag{12}$$

In order to incorporate the buoyancy force and the magnetic force in the model, the total body forces considered the inclined angle can be calculated as follows [42]:

$$F_x=\rho_0g\beta(T-T_m)\sin\lambda+\frac{\mathrm{Ha}^2\mu}{H^2}\left[v\sin\lambda\cos\lambda-u\sin^2\lambda\right]\tag{13}$$

$$F_y=\rho_0g\beta(T-T_m)\cos\lambda+\frac{\mathrm{Ha}^2\mu}{H^2}\left[u\sin\lambda\cos\lambda-v\cos^2\lambda\right]\tag{14}$$

where F_x, F_y are the total body forces at x and y directions, respectively. $\mathrm{Ha}=HB\sqrt{\sigma/\mu}$ is the Hartmann number, in which σ is the electrical conductivity, B is the magnitude of the magnetic field, and H is the length of the cavity. λ is the incline angle. $T_m=(T_h+T_c)/2$ is the average temperature.

The diagonal relaxation matrix $\boldsymbol{S}$ is given by:

$$\boldsymbol{S}=\mathrm{diag}(s_\rho,s_e,s_\varepsilon,s_j,s_q,s_j,s_q,s_v,s_v)\tag{15}$$

The relaxation parameters s_α can be determined by a linear stability analysis. In the present simulation, they are chosen as the following: $s_0=s_3=s_5=1$, $s_1=s_2=1.1$, $s_4=s_6=1.2$ and $s_7=s_8=1/\tau_v$.

When the forcing term is included, the macroscopic fluid velocity is defined as:

$$\boldsymbol{u}=\frac{\sum_i\boldsymbol{e}_if_i}{\rho_0}+\frac{\delta_t\boldsymbol{a}}{2\rho_0}\tag{16}$$

The macroscopic fluid pressure p is defined as:

$$p=\rho_0\frac{5c^2}{48}\left(\sum_{i=1}^{8}f_i+s_0(\boldsymbol{u})\right)\tag{17}$$

3.2. D2Q5-MRT-LBE model for the temperature problem

For the temperature fields, the MRT-LME based on the D2Q5 model is introduced to solve the advection–diffusion, and its equations can be defined as:

$$g_i(\boldsymbol{r}_j+\boldsymbol{e}\delta_t,t+\delta_t)-g_i(\boldsymbol{r}_j,t)=-\boldsymbol{N}^{-1}\boldsymbol{Q}\boldsymbol{N}\left[g_i(\boldsymbol{r}_j,t)-g_i^{eq}(\boldsymbol{r}_j,t)\right]\tag{18}$$

where $g_i(\boldsymbol{r}_j,t)$ is the volume-averaged discrete distribution function with D2Q5 velocity $\boldsymbol{e}_\alpha$ at lattice node r_j, g_i^{eq} is the discrete equilibrium distribution function, $\boldsymbol{N}$ is an orthogonal transformation matrix, and, $\boldsymbol{Q}$ is a diagonal matrix.

The discrete velocities in the D2Q5 model are as follows:

$$e_i=\begin{cases}(0,0), & i=0\\ c\left(\cos\left[(i-1)\frac{\pi}{2}\right],\ \sin\left[(i-1)\frac{\pi}{2}\right]\right), & i=1,2,3,4\end{cases}\tag{19}$$

The transformation matrix $\boldsymbol{N}$ is given by [51]:

$$\boldsymbol{N}=\begin{bmatrix}1&1&1&1&1\\0&1&0&-1&0\\0&0&1&0&-1\\-4&1&1&1&1\\0&1&-1&1&-1\end{bmatrix}\tag{20}$$

For the non-conserved moments, it is assumed that they relax towards the equilibrium $\boldsymbol{n}^{\boldsymbol{eq}}$. Therefore, for the D2Q5 model, the collision process of the MRT method is accomplished as follows:

$$\boldsymbol{n}^{+}=\boldsymbol{n}-\boldsymbol{Q}(\boldsymbol{n}-\boldsymbol{n}^{eq})\tag{21}$$

where $\boldsymbol{n}=\boldsymbol{N}\boldsymbol{g}$. The temperature is the only conserved quantity and is computed by:

$$T\equiv n_0=\sum_{i=0}^{4}g_i\tag{22}$$

And then, the equilibrium moments $\boldsymbol{n}^{eq}=\boldsymbol{N}\boldsymbol{g}^{eq}$ can be constructed accordingly as:

$$n_0^{eq}=T,\quad n_1^{eq}=u_xT,\quad n_2^{eq}=u_yT,\quad n_3^{eq}=AT,\quad n_4^{eq}=0\tag{23}$$

where A is a constant. To avoid the so-called "checkerboard" type numerical instability of the D2Q5 model, the value of A must be smaller than 1 [52]. In this work, A is set to be -2 in simulations. The diagonal relaxation matrix $\boldsymbol{Q}$ is given by:

$$\boldsymbol{Q}=diag(\sigma_0,\sigma_1,\sigma_2,\sigma_3,\sigma_4)\tag{24}$$

In the present simulation, the relaxation parameters are chosen as the following: $\sigma_0=1$, $\sigma_1=\sigma_2=1/\tau_T$, and $\sigma_3=\sigma_4=1.1$.

The streaming step is still carried out in the velocity space by:

$$g_i(\boldsymbol{r}_j+\boldsymbol{e}_i\delta_t,t+\delta_t)=g_i^{+}(\boldsymbol{r}_j,t)\tag{25}$$

where $\boldsymbol{g}^{+}=\boldsymbol{N}^{-1}\boldsymbol{n}^{+}$.

According reference [53], the local equilibrium temperature distribution function can be given by:

$$g_i^{eq}=\overline{w}_iT\left(1+\frac{5\boldsymbol{e}_i\cdot\boldsymbol{u}}{c^2}\right)\tag{26}$$

where the lattice weight coefficients $\overline{w}_i$ are given as follows: $\overline{w_0}=3/5$, $\overline{w}_i=1/10$ for $i=1,2,3,4$.

The kinematical viscosity and the effective thermal diffusivity are given by:

$$v=\frac{1}{3}c^2(\tau_v-0.5)\delta_t\tag{27}$$

$$\alpha=\frac{1}{5}c^2(\tau_T-0.5)\delta_t\tag{28}$$

3.3. Boundary conditions

In the present model, the extrapolation rule for velocity boundary condition is employed to treat the solid/fluid interactions at the walls [32]. The distribution functions on the boundary node x_b are decomposed into equilibrium and non-equilibrium parts:

$$f_i(\boldsymbol{x}_b,t)=\overline{f_i^{eq}}(\boldsymbol{x}_b,t)+\overline{f_i^{neq}}(\boldsymbol{x}_b,t)\tag{29}$$

The non-equilibrium part is approximated by:

$$\overline{f_i^{neq}}(\boldsymbol{x}_b,t)=f_i^{neq}(\boldsymbol{x}_f,t)+O(\delta_t^2)=f_i(\boldsymbol{x}_f,t)-f_i^{eq}(\boldsymbol{x}_f,t)+O(\delta_t^2)\tag{30}$$

where $\boldsymbol{x}_f$ is the nearest neighbor fluid node of $\boldsymbol{x}_b$ along the link $\boldsymbol{e}_i$. The equilibrium part is approximated as follows:

$$\overline{f_i^{eq}}(\boldsymbol{x}_b,t)=f_i^{eq}(p(\boldsymbol{x}_b,t),\boldsymbol{u}(\boldsymbol{x}_b,t))+O(\delta_t\mathrm{Ma}^2)\tag{31}$$

For the velocity boundary condition, the $\boldsymbol{u}(\boldsymbol{x}_b,t)$ is known, but $p(\boldsymbol{x}_b,t)$ is unknown. A modified equilibrium is defined as follows:

$$\overline{f_i^{eq}}(\boldsymbol{x}_b,t) = f_i^{eq}(p(\boldsymbol{x}_f,t),\boldsymbol{u}(\boldsymbol{x}_b,t)) + O(\delta_t \mathrm{Ma}^2) \tag{32}$$

The discrete distribution function $f_i(x_b,t)$ at the boundary node x_b is calculated as:

$$f_i(\boldsymbol{x}_b,t) = \overline{f_i^{eq}}(\boldsymbol{x}_b,t) + f_i(\boldsymbol{x}_f,t) - f_i^{eq}(\boldsymbol{x}_f,t) \tag{33}$$

which has the accuracy of $O(\delta_t^2 + \delta_t \mathrm{Ma}^2)$.

The corresponding thermodynamic boundary conditions with second order accuracy are implemented in the similar way. The discrete temperature distribution on the boundary is given by:

$$g_i(\boldsymbol{x}_b,t) = \overline{g_i^{eq}}(\boldsymbol{x}_b,t) + g_i(\boldsymbol{x}_f,t) - g_i^{eq}(\boldsymbol{x}_f,t) \tag{34}$$

The temperature on the boundary node can be approximated by:

$$T(\boldsymbol{x}_b,t) = \frac{4T(\boldsymbol{x}_f,t) - T(\boldsymbol{x}_{ff},t) - 2\Delta\boldsymbol{x}\cdot\nabla T(\boldsymbol{x}_b,t)}{3} \tag{35}$$

where $\Delta\boldsymbol{x} = \boldsymbol{x}_f - \boldsymbol{x}_b = \boldsymbol{x}_{ff} - \boldsymbol{x}_f$ ($\boldsymbol{x}_{ff}$ is the nearest fluid node of $\boldsymbol{x}_f$ along the link $\boldsymbol{e}_i$).

3.4. Governing parameters

The non-dimensional parameters are the Prandtl number Pr and the Rayleigh number Ra defined by:

$$\mathrm{Pr} = \frac{\nu}{\alpha} \tag{36}$$

$$\mathrm{Ra} = \frac{g\beta\Delta T H^3}{\nu\alpha} \tag{37}$$

where $\Delta T = T_h - T_c$ is the reference temperature difference.

The Mach number is defined as $\mathrm{Ma} = u_0/c_s$, where $u_0 = \sqrt{g\beta\Delta T H}$ and $c_s = c/\sqrt{3}$ which are the characteristic velocity and the sound speed of the lattice fluid, respectively. In the standard LBM, the lattice speed c is often set to be 1 with $\delta_x = \delta_t = 1$. Thus, when the Prandtl number and the Rayleigh number are specified, the Mach number is directly proportional to τ_v and inversely proportional to H. Sheikholeslami et al. [30] found that the average Nusselt number varies even for a same lattice numbers if Mach number changes at a constant Rayleigh number. So Mach number should have a constant value similar to other parameters for all calculations to cover a steady solving. To comply with the incompressible limit of the flow, the Mach number should be $\mathrm{Ma} < 0.3$. Unless otherwise specified, the Mach number is fixed at $\mathrm{Ma} = 0.1$ in the present work, and then the non-dimensional relaxation times are defined by:

$$\tau_v = \frac{1}{2} + \frac{\mathrm{Ma}H\sqrt{3\mathrm{Pr}}}{c\delta_t\sqrt{\mathrm{Ra}}} \tag{38}$$

$$\tau_T = \frac{1}{2} + \frac{5(\tau_v - 0.5)}{3\mathrm{Pr}} \tag{39}$$

3.5. Lattice Boltzmann method for nanofluids

The dynamical similarity depends on three dimensionless parameters: the Prandtl number Pr, the Rayleigh number Ra, and the Mach number Ma. The nanofluids have a unique feature which is quite different from those of the convectional solid–liquid mixtures in which millimeter and/or micrometer-sized particles are added. The nanofluid is a solid–liquid mixture in which metallic or nonmetallic nanoparticles are suspended and behaves more like a fluid rather than a conventional solid–fluid mixture. So, the nanofluid can be assumed to be a pure fluid. And then, the nanofluid qualities are obtained. The properties of the nanofluid are assumed to be constant except for the density variation, which is approximated by the Boussinesq model.

Table 1
Thermal-physical properties of pure water and Cu.

Property	Pure water	Cu
ρ (kg m^{-3})	997	8954
C_P (J kg^{-1} K^{-1})	4179	383
β (K^{-1})	0.00021	0.00000167
k (W m^{-1} K^{-1})	0.613	400
μ (kg m^{-1} s^{-1})	0.000855	

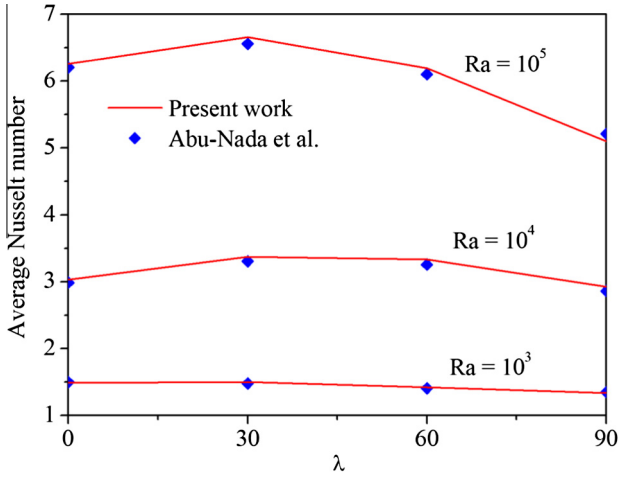

Fig. 2. Validation of the present simulation against Abu-Nada and Oztop.

Table 2
Comparison of the present numerical results with the reported data in literature [60].

Ha	$\mathrm{Gr} = 2\times10^4$		$\mathrm{Gr} = 2\times10^5$	
	Present	Rudraiah et al.	Present	Rudraiah et al.
0	2.52285	2.5188	5.07702	4.9198
10	2.23118	2.2234	4.96846	4.8053
50	1.08412	1.0856	2.99103	2.8442
100	1.00647	1.0110	1.45786	1.4317

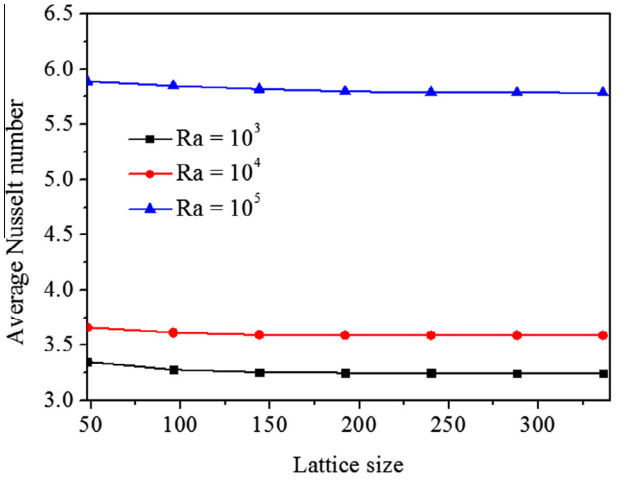

Fig. 3. Effect of grid size on the average Nusselt number at the cold wall.

The density of the nanofluid is given by:

$$\rho_{nf} = (1-\varphi)\rho_f + \varphi\rho_p \tag{40}$$

where φ refers to the volume fraction of nanoparticles and the subscripts *nf*, *f*, *p* denote the nanofluid, the base fluid and the particle, respectively.

By assuming a thermal equilibrium between the particles and the surrounding fluid, the specific heat is obtained as:

$$(\rho C_P)_{nf} = (1-\varphi)(\rho C_P)_f + \varphi(\rho C_P)_p \tag{41}$$

The thermal expansion coefficient of the nanofluid can be determined by:

$$(\rho\beta)_{nf} = (1-\varphi)(\rho\beta)_f + \varphi(\rho\beta)_p \tag{42}$$

The thermal diffusivity of the nanofluid is:

$$\alpha_{nf} = \frac{k_{nf}}{(\rho C_P)_{nf}} \tag{43}$$

The Maxwell–Garnetts model [54] was used to calculate the effective thermal conductivity of the nanofluid:

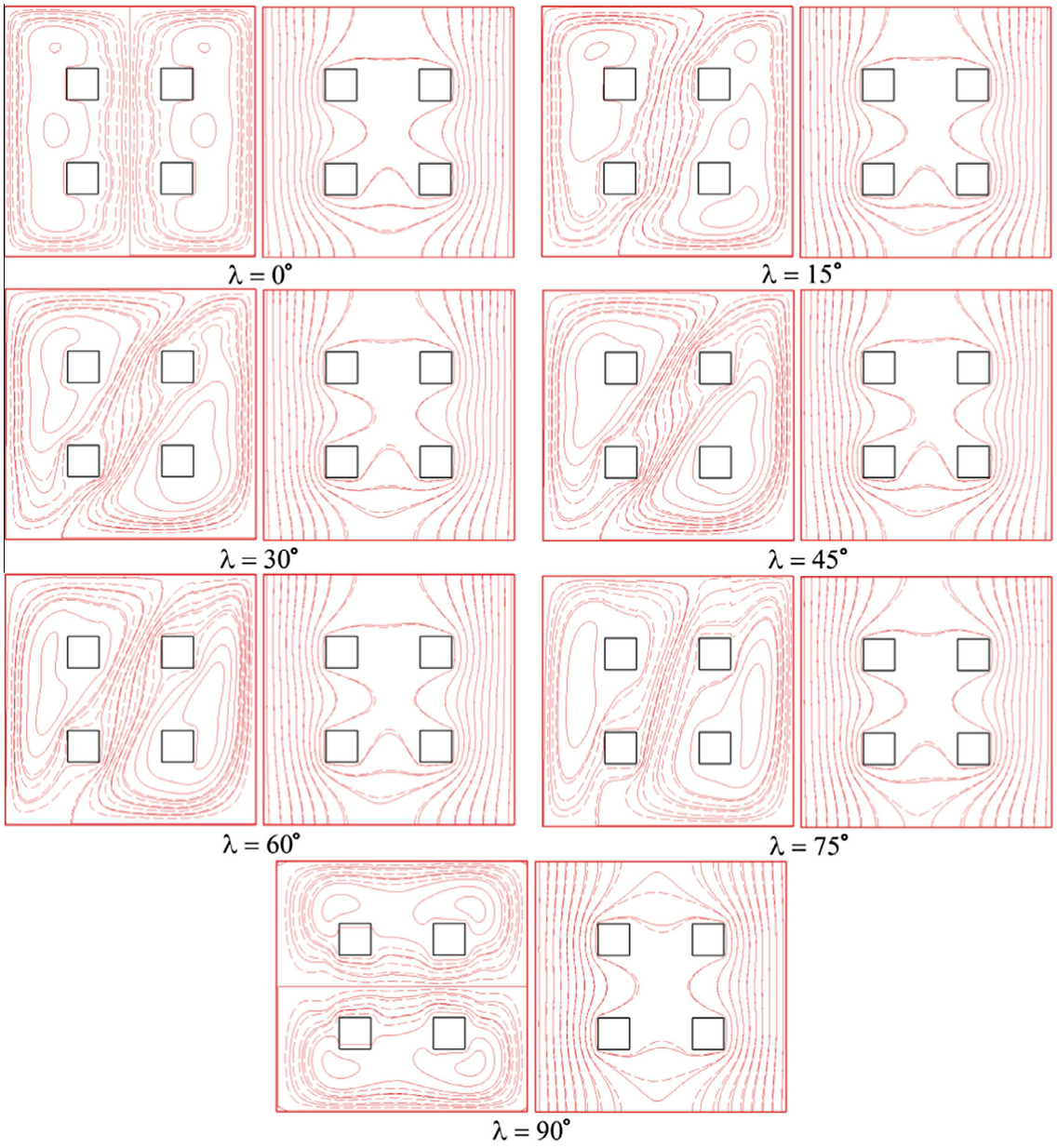

Fig. 4. Streamlines and isotherms at different inclination angles for Ra = 10^5 and $\varphi = 0.1$ (—: nanofluid and – –: water).

Table 3
Maximum stream function for different inclination angles with Ra = 10^5 and $\varphi = 0.1$.

Property	$\lambda = 0°$	$\lambda = 15°$	$\lambda = 30°$	$\lambda = 45°$	$\lambda = 60°$	$\lambda = 75°$	$\lambda = 90°$
Pure water	1940	−2238	−2561	−2992	−3315	−3329	2006
Nanofluid	3619	−4162	−4806	−5607	−6194	−6167	3750

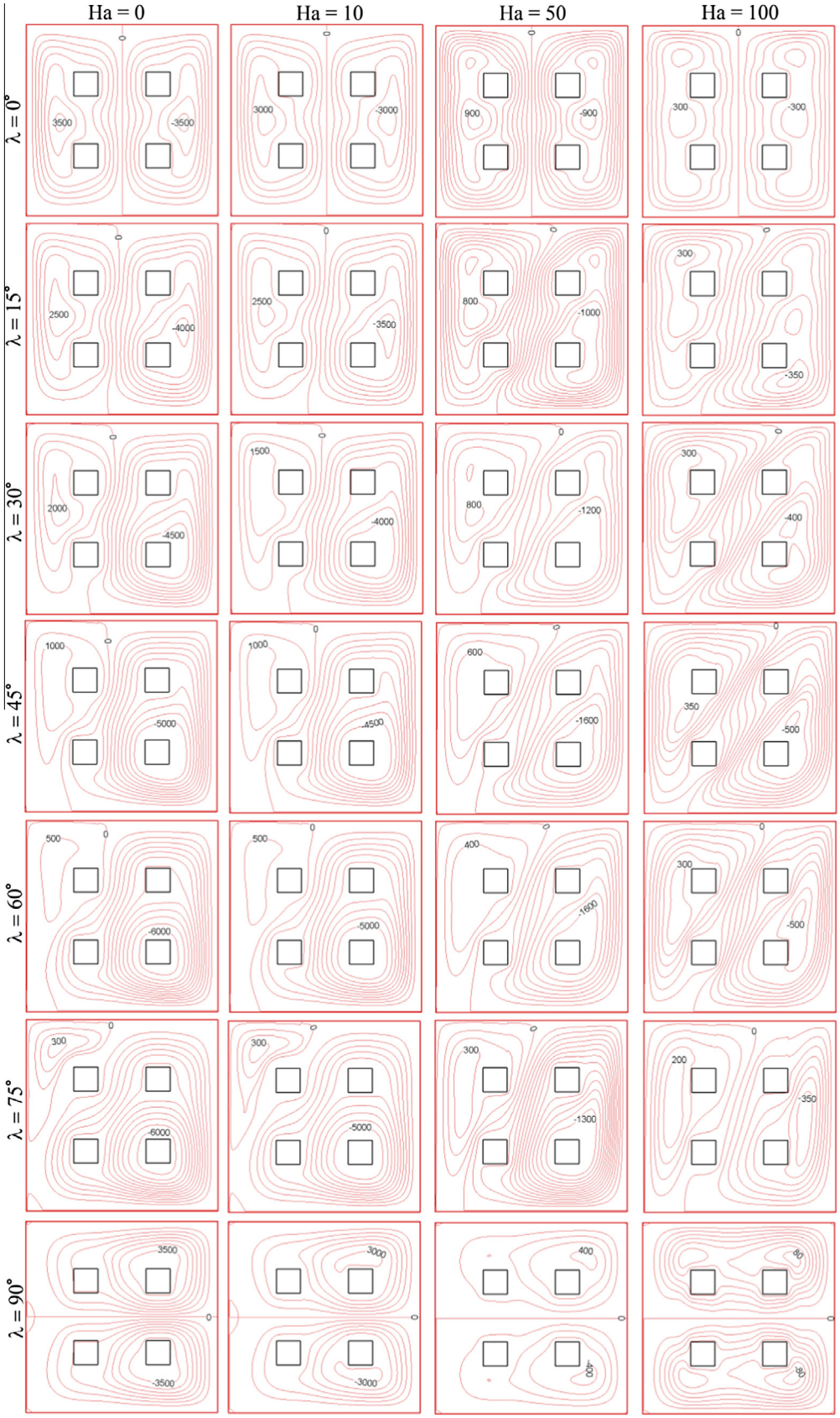

Fig. 5. Streamlines for different inclination angles and Hartmann numbers with Ra = 10^5 and $\varphi = 0.1$.

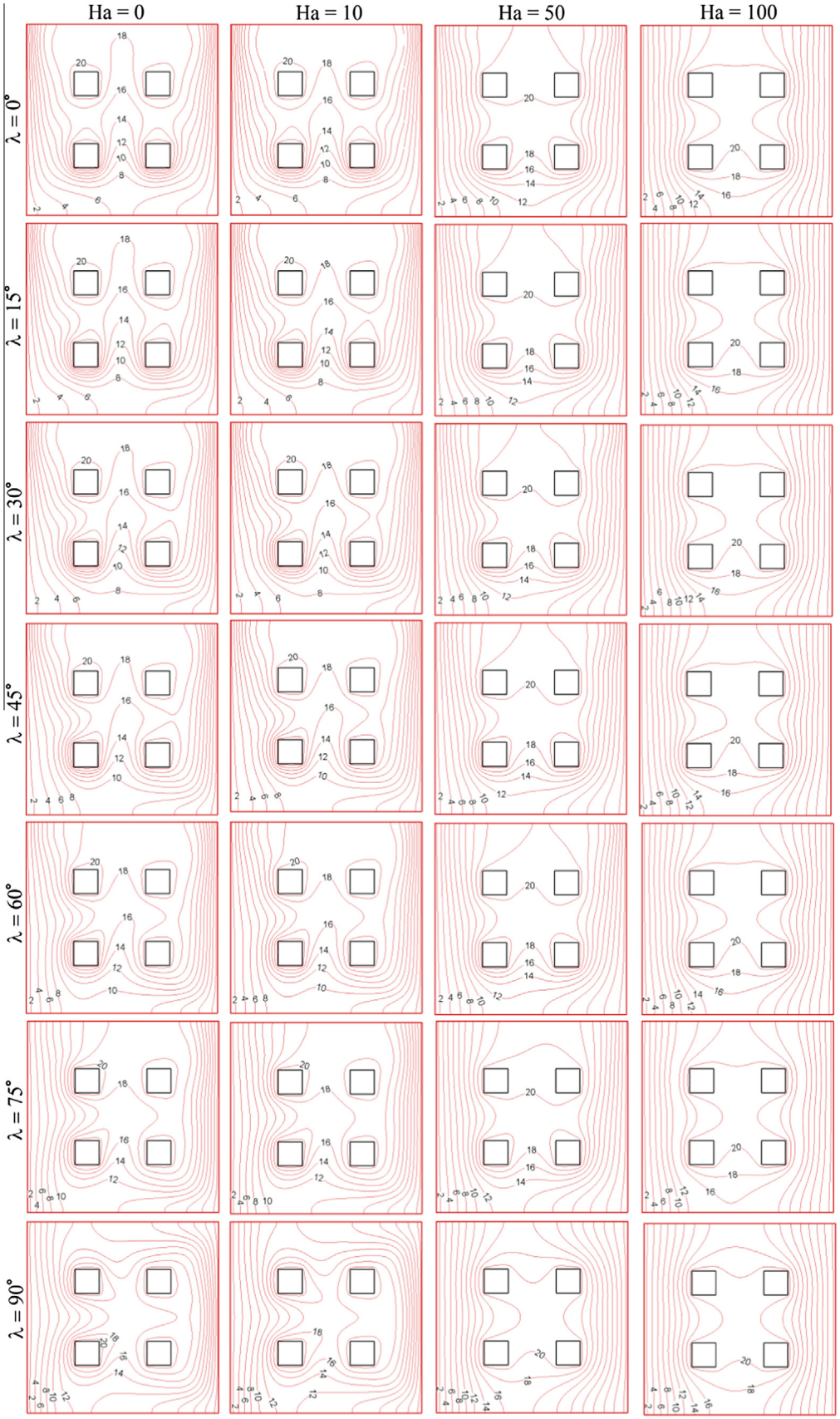

Fig. 6. Isotherms for different inclination angles and Hartmann numbers with Ra = 10^5 and $\varphi = 0.1$.

$$\frac{k_{nf}}{k_f} = \frac{k_p + 2k_f - 2\varphi(k_f - k_p)}{k_p + 2k_f + \varphi(k_f - k_p)} \tag{44}$$

The use of Eq. (44) is restricted to spherical nanoparticles where the nanoparticles of other shapes are not taken into account. According to reference [55–57], this model is found to be appropriate for studying heat transfer enhancement using nanofluids.

The viscosity of the nanofluid can be approximated as [58]:

$$\mu_{nf} = \frac{\mu_f}{(1-\varphi)^{2.5}} \tag{45}$$

The Nusselt number is a measure of heat transfer ratio of natural convection. The local Nusselt number and the average Nusselt number are defined, respectively by:

$$\mathrm{Nu} = -\frac{k_{nf}}{k_f}\frac{H}{\Delta T}\left(\frac{\partial T}{\partial x}\right)_{\mathrm{w}} \tag{46}$$

$$\mathrm{Nu}_{\mathrm{ave}} = \frac{1}{H}\int_0^H \mathrm{Nu}dy \tag{47}$$

where the temperature gradient $\partial T/\partial x$ is calculated using five points formula.

The corresponding thermal-physical properties of the based fluid and the nanoparticles are shown in Table 1.

4. Code validation and grid independence

The validation of the computations is very important in the numerical study. Two test cases were performed to validate the accuracy of the present numerical solution. The first benchmark solution for nanofluids natural convection in an inclined square cavity was published by Abu-Nada and Oztop [59]. They employed a two-dimensional enclosure for which two walls were maintained at different constant temperatures and the other two walls were thermally insulated. Fig. 2 presents the variation of the average Nusselt number along the hot wall versus inclination angle at different Rayleigh numbers and excellent agreement is achieved. Another test of the validation was verified against the existing results for natural convection inside the square enclosure in the presence of an external magnetic field. As shown in Table 2, a good comparison of the present results with the benchmark solution of Rudraiah et al. [60] is observed.

In order to determine a proper grid for the final computations, Grid-independence examination was conducted for the natural convection heat transfer in the square cavity as shown in Fig. 1. Seven different lattice sizes, 48×48, 96×96, 144×144, 192×192, 240×240, 288×288, and 336×336 were employed to validate the solution independency of the grid number. Fig. 3 shows the variation of the average Nusselt number over the cold wall with the different grid sizes. It is observed that an 192×192 uniform grid can be considered as a grid-independent one for the Rayleigh number $\mathrm{Ra}=10^4$. Through the same method, the lattice sizes of 144×144 for $\mathrm{Ra}=10^3$, and 240×240 for $\mathrm{Ra}=10^5$, were obtained, respectively.

5. Results and discussion

Numerical simulations are performed to investigate the fluid flow and heat transfer of water-based nanofluids in an inclined square cavity with four heat sources in the presence of the magnetic field. The computations are carried out for a wide range of Rayleigh numbers ($\mathrm{Ra}=10^3$, 10^4 and 10^5), Hartmann numbers ($\mathrm{Ha}=0$, 10, 50 and 100), inclination angles ($0^\circ\leqslant\lambda\leqslant90^\circ$ with $\Delta\lambda=15^\circ$), and volume fractions of nanoparticles ($\varphi=0.03$, 0.07 and 0.1). The streamlines, isotherms, local and average Nusselt numbers are presented for various values of pertinent parameters involved in the study.

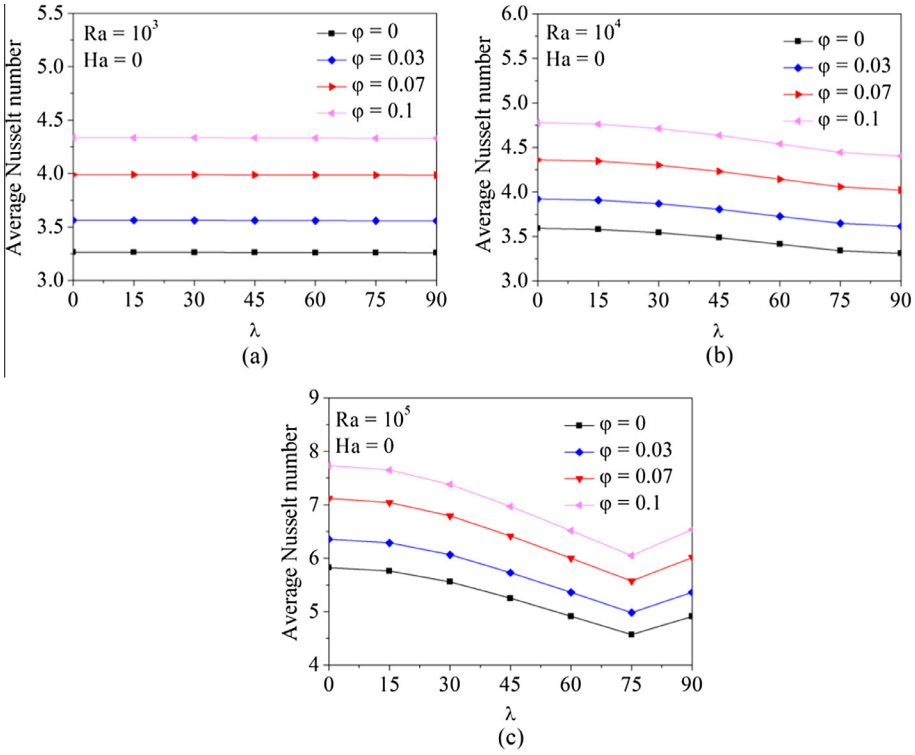

Fig. 7. Average Nusselt number at the cold wall versus inclination angle for different Rayleigh numbers.

5.1. Flow and temperature fields

Fig. 4 presents the streamlines and isotherms in the enclosure for different nanoparticles volume fractions ($\varphi = 0$ and $\varphi = 0.1$) and inclination angles ($\lambda = 0^\circ$, 15°, 30°, 45°, 60°, 75°, and 90°) in the absence of a magnetic field. The Rayleigh number is $Ra = 10^5$. The larger absolute values of the stream function are detected for the nanofluid compared to that for the pure water, and this indicates that the strength of the circulation increases with an increase in the nanoparticles volume fraction at a particular inclination angle. Similar trend can be found in Table 3 by comparing the magnitude of the maximum stream function for the pure water with that for the Cu–water nanofluid. The high energy of irregular motion of nanoparticles in the fluid explains the higher streamline intensity, which in turn enhances the heat transfer process of the nanofluid in the square cavity. Moreover, the temperature gradient of the nanofluid near the cold surface is similar to that of the pure water. This demonstrates that the temperature gradient has very small influence on the Nusselt number according to Eq. (29). However, since the effect of the ratio of nanofluid conductivity to water conductivity, k_{nf}/k_f, is more pronounced than the effect of temperature gradient, and the enhancement of heat transfer is observed with the addition of nanoparticles in the following discussions.

Figs. 5 and 6 respectively show the streamlines and the isotherms in the enclosure filled with the Cu–water nanofluid at different inclination angles and Hartmann numbers. The Rayleigh number is $Ra = 10^5$ and the nanoparticles volume fraction is $\varphi = 0.1$. When $\lambda = 0^\circ$, the enclosure is placed horizontally and the buoyancy force acts only in the y-direction. The flow domain and the boundary conditions are symmetrical, and then the streamlines and the isotherms are symmetric with respect to the vertical centerline of the square cavity. At low Hartmann numbers ($Ha = 0$ and $Ha = 10$), two symmetrical counter-rotating vortices, a counterclockwise and a clockwise, are generated within the square cavity. As the Hartmann number increases ($Ha = 50$), two small symmetrical circulation cells begin to form in the upper portion of the square cavity near the out corner of the heat sources. With further increase of the Hartmann number ($Ha = 100$), two another secondary symmetrical eddies start to develop in the bottom portion of the square cavity near the out corner of the heat

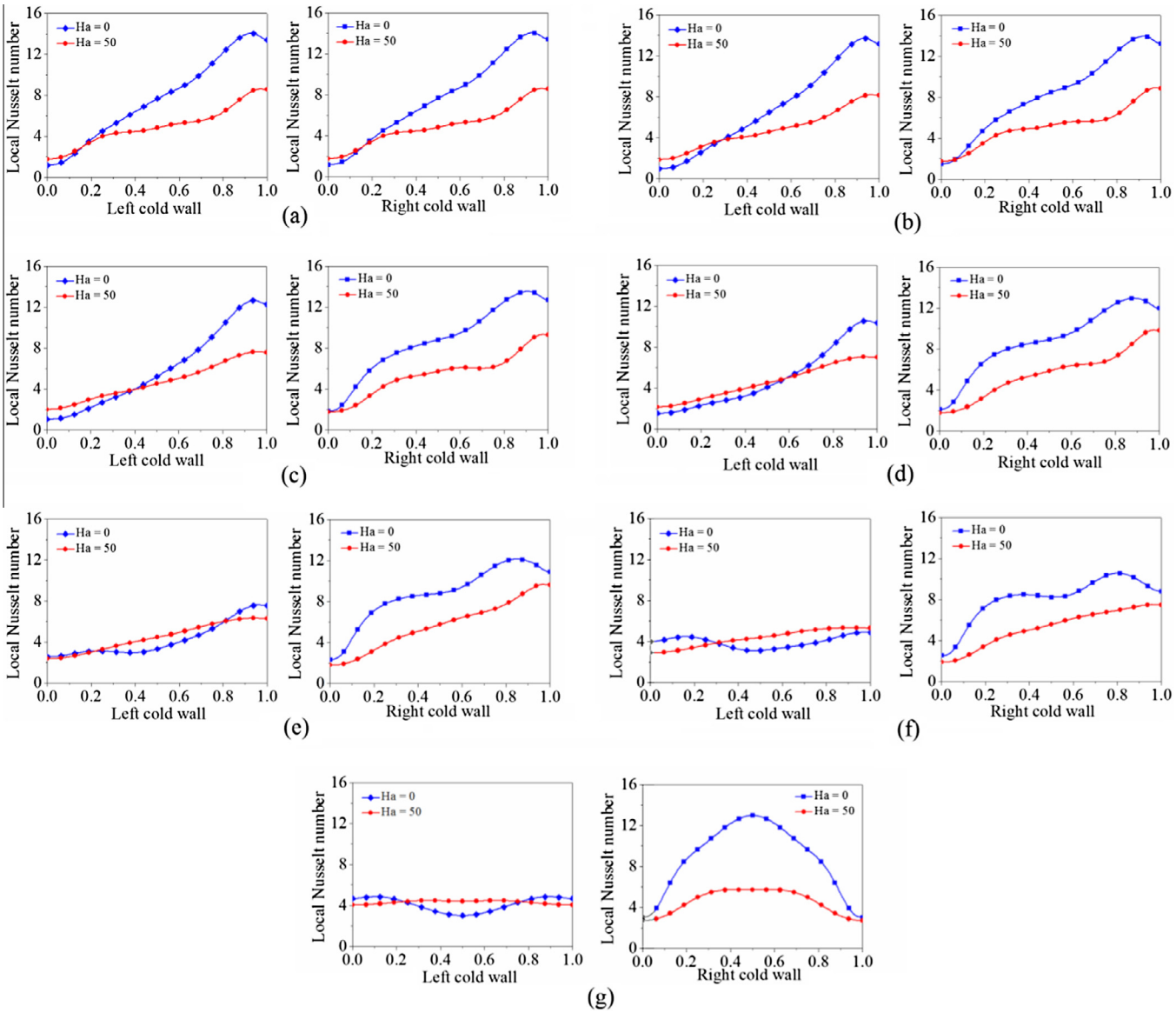

Fig. 8. Local Nusselt number along the cold wall for different inclination angles. (a) $\lambda = 0^\circ$, (b) $\lambda = 15^\circ$, (c) $\lambda = 30^\circ$, (d) $\lambda = 45^\circ$, (e) $\lambda = 60^\circ$, (f) $\lambda = 75^\circ$, and (g) $\lambda = 90^\circ$.

sources. The inclination angle has a remarkable effect on the flow patterns for all values of Hartmann numbers. For Ha = 0 and Ha = 10, the left initial anticlockwise vortex is squeezed thinner and dragged to the up left part of the enclosure while the primary clockwise starts to develop towards the left bottom part of the cavity as the inclination angle increases from $\lambda = 15^\circ$ to $\lambda = 75^\circ$. At $\lambda = 90^\circ$, the primary two counter-rotating vortices become symmetrical again with respect to the horizontal centerline of the square cavity in the *x*-direction. For Ha = 50 and Ha = 100, the initial two large counter-rotating vortices are quite similar to those for low Hartmann numbers as the inclination angle increases from $\lambda = 15^\circ$ to $\lambda = 90^\circ$. While the initial two secondary vortices start to die out as the inclination angle increases from $\lambda = 15^\circ$ to $\lambda = 75^\circ$, and again develop at $\lambda = 90^\circ$. The inclination angle also has a noticeable effect on the formation of the isotherms for low Hartmann numbers. However, for High Hartmann numbers, this effect becomes marginal as can be seen in Fig. 6. Moreover, the strength of the circulation patterns in the enclosure becomes weaker as the magnetic intensity becomes stronger at any given inclined angle. This can clearly be demonstrated by the values of the stream function in Fig. 5. Hence, the intensity of convection decreases significantly as the Hartmann number increases, which indicating a lower heat transfer rate.

5.2. Heat transfer rate

Caculations of the heat transfer rate across the enclosure is very important in engineering applications. In order to find the effect of the nanoparticles volume fraction, the Rayleigh number and the inclination angle on the heat transfer rate, the variations of the average Nusselt number along the cold wall as a function of inclination angle λ at different values of nanoparticles volume fraction and Rayleigh numbers are presented in Fig. 7. In general, the results show that the average Nusselt number increases as the Rayleigh number increases due to the strengthened buoyant flow. The average Nusselt number is lower for the enclosure filled with pure water than that filled with the Cu–water nanofluid for any given Rayleigh number and inclination angle considered in this paper. This is an indication of improvement in the heat transfer performance as a result of adding nanoparticles into the base fluid. Fig. 7 also presents the effect of the inclination angle on the average Nusselt number. For the low Rayleigh number ($Ra = 10^3$), where the viscous force is greater than the buoyancy force, there is no discernible influence of the inclination angle on the average Nusselt number, as expected, since the dominant energy transport mechanism is mainly due to conduction. As the Rayleigh number increases to $Ra = 10^4$, the average Nusselt number generally decreases with increasing the inclination angle and reaches its minimum value at $\lambda = 90^\circ$. This reduction can be explained by that the major heat transfer mechanism in the cavity shifts from the conduction mode to the convective mode and the buoyancy force is reduced by a factor of the inclination angle. However, the average Nusselt number decreases at first as the inclination angle increases and reaches a minimum at a specific inclination angle, around $\lambda = 75^\circ$ at $Ra = 10^5$, then increases with increasing the inclination angle to $\lambda = 90^\circ$. The reason is that the convective is the principal mode of the heat transfer and the convection intensity is very strong. The temperature contours are compressed towards the right cold wall, as can be seen in Fig. 6, which in turn results in a larger heat transfer rate at $\lambda = 90^\circ$.

Fig. 8 shows the distributions of the local Nusselt number along the cold wall in the inclined cavity for different Hartmann numbers and inclination angles. The volume fraction of nanoparticles is $\varphi = 0.1$ and the Rayleigh number is $Ra = 10^5$. The results show that the Hartmann number has a significant effect on the local Nusselt number distribution patterns along the cold wall. Also, it is found that the initial maximum of the local Nusselt number at the cold wall is parentally decreased as the Hartmann number increases from Ha = 0 to Ha = 50 for any given inclination angle

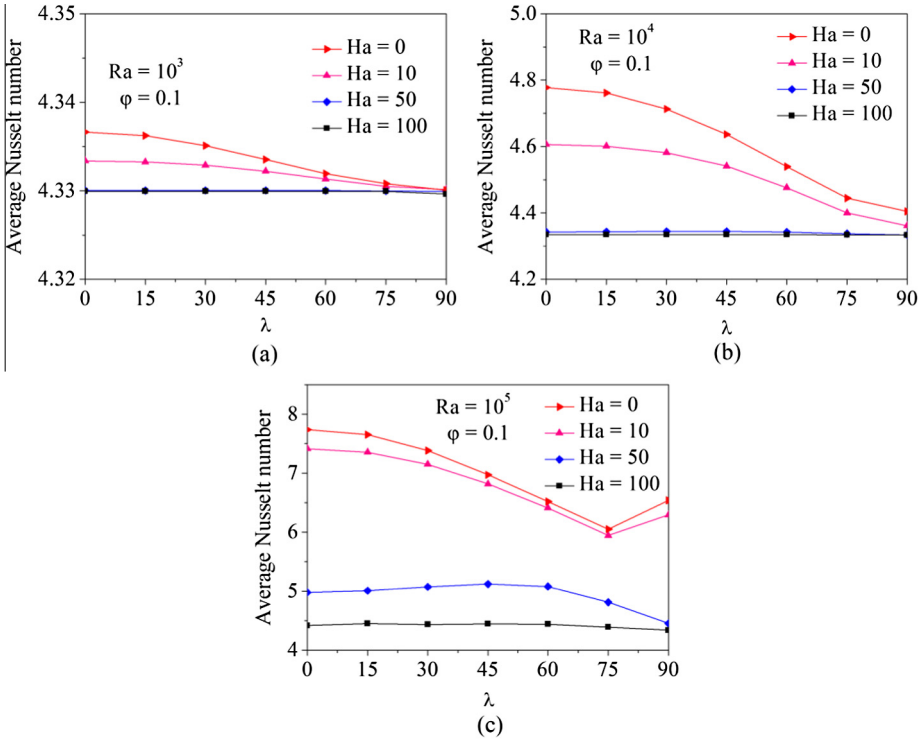

Fig. 9. Average Nusselt number at the cold wall versus inclination angle λ for different Rayleigh numbers.

in this study. This is because that the high values of the stream function (i.e., high flow rate) are suppressed by the stronger magnetic field in the cavity.

The effects of Hartmann numbers and Rayleigh numbers on the average Nusselt number at the cold wall are displayed in Fig. 9. It is observed that the average Nusselt number is lower for the square cavity in the presence of the magnetic field than that for the enclosure in the absence of the magnetic field at any given Rayleigh number and inclination angle. For $Ha = 0$ and $Ha = 10$, the average Nusselt number is decreased as the inclination angle increases when $Ra = 10^3$ and $Ra = 10^4$. And for $Ra = 10^5$, the average Nusselt number decreases at first as the inclination angle increases and reaches a minimum at a specific inclination angle, and then increases with increasing the inclination angle to $\lambda = 90^\circ$. As the Hartmann number increases to $Ha = 50$, the average Nusselt number increases at first as the inclination angle increases and reaches a maximum at around $\lambda = 45^\circ$, and then decreases with increasing the inclination angle to $\lambda = 90^\circ$ for $Ra = 10^5$. This is because that the fluid velocities are considerable and the heat transfer is mainly due to convection, the influence of the magnetic field on the heat transfer process becomes considerable. The intensity of isotherms in the vicinity of the vertical walls decreases as the Hartmann number increases, which results in a lower heat transfer rate. With further increasing the Hartmann number ($Ha = 100$), the inclination angle dose not have a considerable effect on the average Nusselt number for all values of Rayleigh numbers. This can be explained by that the effect of the magnetic field on the heat transfer rate becomes stronger, which results in a significant reduction of the heat transfer.

6. Conclusions

In this work, magneto-hydrodynamic (MHD) flow and heat transfer of Cu–water nanofluids in an inclined square enclosure with four heat sources were numerically studied using the double multiple-relaxation-time (MRT) thermal lattice Boltzmann method. The flow and temperature fields were solved with the D2Q9-MRT and D2Q5-MRT model, respectively. The present solutions are well validated in comparisons with previous numerical investigations, and consequently the MRT lattice Boltzmann method is competent for solving heat transfer performance of nanofluids in enclosures that is influenced by a magnetic field. The effects of the inclination angle, the Rayleigh number, the volume fraction of nanoparticles, and the Hartmann number on the fluid flow and heat transfer of the cavity were investigated. From the results presented above, the following main conclusions can be drawn.

The addition of nanoparticles of Cu into the base fluid is more effective on the flow fields than on the temperature distributions. The enclosure with nanofluids exhibits a remarkable enhancement heat transfer compared to that with the pure water. The average Nusselt number increases significantly with the increase of volume fraction of nanoparticles for all values of Rayleigh numbers.

The inclination angle has a significant impact on the flow fields, the temperature patterns, and the local Nusselt Number distributions. The average Nusselt number decreases at first as the inclination angle increases and reaches a minimum at a specific inclination angle, around $\lambda = 75^\circ$, and then increases with further increasing the inclination angle to $\lambda = 90^\circ$ at $Ra = 10^5$.

The heat transfer rate is suppressed in the presence of a magnetic field for all values of Rayleigh numbers and inclination angles. Moreover, when $Ra = 10^5$, the average Nusselt number increases at first as the inclination angle increases and reaches a maximum at a certain inclination angle, and then decreases with the inclination angle further increased at $Ha = 50$. As the Hartmann number increases to $Ha = 100$, the inclination angle shows have a inconsiderable effect on the average Nusselt number for all values of Rayleigh numbers.

References

[1] K.-O. Lim, K.-S. Lee, T.-H. Song, Primary and secondary instabilities in a glass-melting surface, Numer. Heat Transfer A 36 (1999) 309–325.
[2] P.O. Iwanik, W.K. Chiu, Temperature distribution of an optical fiber traversing through a chemical vapor deposition reactor, Numer. Heat Transfer A 43 (2003) 221–237.
[3] S.-W. Kang, W.-C. Wei, S.-H. Tsai, C.-C. Huang, Experimental investigation of nanofluids on sintered heat pipe thermal performance, Appl. Therm. Eng. 29 (2009) 973–979.
[4] V.I. Polezhaev, M.N. Myakshina, S.A. Nikitin, Heat transfer due to buoyancy-driven convective interaction in enclosures: fundamentals and applications, Int. J. Heat Mass Transfer 55 (2012) 156–165.
[5] T. Basak, S. Roy, A. Balakrishnan, Effects of thermal boundary conditions on natural convection flows within a square cavity, Int. J. Heat Mass Transfer 49 (2006) 4525–4535.
[6] N.H. Saeid, Y. Yaacob, Natural convection in a square cavity with spatial side-wall temperature variation, Numer. Heat Transfer A 49 (2006) 683–697.
[7] Q.-H. Deng, J.-J. Chang, Natural convection in a rectangular enclosure with sinusoidal temperature distributions on both side walls, Numer. Heat Transfer A 54 (2008) 507–524.
[8] Y. Xuan, Q. Li, Heat transfer enhancement of nanofluids, Int. J. Heat Fluid Flow 21 (2000) 58–64.
[9] W. Daungthongsuk, S. Wongwises, A critical review of convective heat transfer of nanofluids, Renewable Sustainable Energy Rev. 11 (2007) 797–817.
[10] X.-Q. Wang, A.S. Mujumdar, Heat transfer characteristics of nanofluids: a review, Int. J. Therm. Sci. 46 (2007) 1–19.
[11] S.K. Das, S.U. Choi, H.E. Patel, Heat transfer in nanofluids-a review, Heat Transfer Eng. 27 (2006) 3–19.
[12] K.S. Hwang, J.-H. Lee, S.P. Jang, Buoyancy-driven heat transfer of water-based Al_2O_3 nanofluids in a rectangular cavity, Int. J. Heat Mass Transfer 50 (2007) 4003–4010.
[13] R.-Y. Jou, S.-C. Tzeng, Numerical research of nature convective heat transfer enhancement filled with nanofluids in rectangular enclosures, Int. Commun. Heat Mass Transfer 33 (2006) 727–736.
[14] K. Khanafer, K. Vafai, M. Lightstone, Buoyancy-driven heat transfer enhancement in a two-dimensional enclosure utilizing nanofluids, Int. J. Heat Mass Transfer 46 (2003) 3639–3653.
[15] C.-J. Ho, M. Chen, Z. Li, Numerical simulation of natural convection of nanofluid in a square enclosure: effects due to uncertainties of viscosity and thermal conductivity, Int. J. Heat Mass Transfer 51 (2008) 4506–4516.
[16] A. Nnanna, Experimental model of temperature-driven nanofluid, J. Heat Transfer 129 (2007) 697–704.
[17] B. Ghasemi, S. Aminossadati, Natural convection heat transfer in an inclined enclosure filled with a water–Cuo nanofluid, Numer. Heat Transfer A 55 (2009) 807–823.
[18] E. Abu-Nada, H.F. Oztop, Numerical analysis of Al_2O_3/water nanofluids natural convection in a wavy walled cavity, Numer. Heat Transfer A 59 (2011) 403–419.
[19] M. Akhtari, M. Haghshenasfard, M. Talaie, Numerical and experimental investigation of heat transfer of α-Al_2O_3/water nanofluid in double pipe and shell and tube heat exchangers, Numer. Heat Transfer A 63 (2013) 941–958.
[20] E. Sourtiji, D. Ganji, M. Gorji-Bandpy, S. Seyyedi, Numerical study of periodic natural convection in a nanofluid-filled enclosure due to transitional temperature of heat source, Powder Technol. 259 (2014) 65–73.
[21] O. Pourmehran, M. Rahimi-Gorji, M. Gorji-Bandpy, D. Ganji, Analytical investigation of squeezing unsteady nanofluid flow between parallel plates by LSM and CM, Alexandria Eng. J. 54 (2015) 17–26.
[22] O. Pourmehran, M. Rahimi-Gorji, M. Hatami, S. Sahebi, G. Domairry, Numerical optimization of microchannel heat sink (MCHS) performance cooled by KKL based nanofluids in saturated porous medium, J. Taiwan Inst. Chem. Eng. 55 (2015) 49–68.
[23] M. Rahimi-Gorji, O. Pourmehran, M. Gorji-Bandpy, D. Ganji, An analytical investigation on unsteady motion of vertically falling spherical particles in non-newtonian fluid by collocation method, Ain Shams Eng. J. 6 (2015) 531–540.
[24] M. Rahimi-Gorji, O. Pourmehran, M. Hatami, D. Ganji, Statistical optimization of microchannel heat sink (MCHS) geometry cooled by different nanofluids using RSM analysis, Eur. Phys. J. Plus 130 (2015) 1–21.
[25] I. Rashidi, O. Mahian, G. Lorenzini, C. Biserni, S. Wongwises, Natural convection of Al_2O_3/water nanofluid in a square cavity: effects of heterogeneous heating, Int. J. Heat Mass Transfer 74 (2014) 391–402.
[26] M. Sathiyamoorthy, A. Chamkha, Effect of magnetic field on natural convection flow in a liquid gallium filled square cavity for linearly heated side wall(s), Int. J. Therm. Sci. 49 (2010) 1856–1865.
[27] I. Mejri, A. Mahmoudi, M.A. Abbassi, A. Omri, Magnetic field effect on entropy generation in a nanofluid-filled enclosure with sinusoidal heating on both side walls, Powder Technol. 266 (2014) 340–353.

[28] S. Aminossadati, B. Ghasemi, A. Kargar, Computational analysis of magnetohydrodynamic natural convection in a square cavity with a thin fin, Eur. J. Mech.-B/Fluids 46 (2014) 154–163.
[29] G. Bourantas, V. Loukopoulos, MHD natural-convection flow in an inclined square enclosure filled with a micropolar-nanofluid, Int. J. Heat Mass Transfer 79 (2014) 930–944.
[30] F. Selimefendigil, H.F. Öztop, Numerical study of MHD mixed convection in a nanofluid filled lid driven square enclosure with a rotating cylinder, Int. J. Heat Mass Transfer 78 (2014) 741–754.
[31] Q. Li, Y. He, Y. Wang, G. Tang, An improved thermal lattice Boltzmann model for flows without viscous heat dissipation and compression work, Int. J. Mod. Phys. C 19 (2008) 125–150.
[32] Z. Guo, B. Shi, C. Zheng, A coupled lattice BGK model for the Boussinesq equations, Int. J. Numer. Methods Fluids 39 (2002) 325–342.
[33] X. He, L.-S. Luo, Lattice Boltzmann model for the incompressible Navier–Stokes equation, J. Stat. Phys. 88 (1997) 927–944.
[34] Q. Zou, S. Hou, S. Chen, G.D. Doolen, A improved incompressible lattice Boltzmann model for time-independent flows, J. Stat. Phys. 81 (1995) 35–48.
[35] Z. Lin, H. Fang, R. Tao, Improved lattice Boltzmann model for incompressible two-dimensional steady flows, Phys. Rev. E 54 (1996) 6323.
[36] Z. Guo, B. Shi, N. Wang, Lattice BGK model for incompressible Navier–Stokes equation, J. Comput. Phys. 165 (2000) 288–306.
[37] Y. Xuan, Z. Yao, Lattice Boltzmann model for nanofluids, Heat Mass Transfer 41 (2005) 199–205.
[38] H. Nemati, M. Farhadi, K. Sedighi, E. Fattahi, A. Darzi, Lattice Boltzmann simulation of nanofluid in lid-driven cavity, Int. Commun. Heat Mass Transfer 37 (2010) 1528–1534.
[39] H. Sajjadi, M. Gorji, G. Kefayati, D. Ganji, Lattice Boltzmann simulation of turbulent natural convection in tall enclosures using Cu/water nanofluid, Numer. Heat Transfer 62 (2012) 512–530.
[40] G.R. Kefayati, Simulation of ferrofluid heat dissipation effect on natural convection at an inclined cavity filled with kerosene/cobalt utilizing the Lattice Boltzmann method, Numer. Heat Transfer 65 (2014) 509–530.
[41] T. Zhang, D. Che, Lattice Boltzmann simulation of natural convection in an inclined square cavity with spatial temperature variation, Numer. Heat Transfer A 66 (2014) 712–732.
[42] G.R. Kefayati, Lattice Boltzmann simulation of MHD natural convection in a nanofluid-filled cavity with sinusoidal temperature distribution, Powder Technol. 243 (2013) 171–183.
[43] M. Sheikholeslami, M. Gorji-Bandpy, Free convection of ferrofluid in a cavity heated from below in the presence of an external magnetic field, Powder Technol. 256 (2014) 490–498.
[44] M. Sheikholeslami, M. Gorji-Bandpy, K. Vajravelu, Lattice Boltzmann simulation of magnetohydrodynamic natural convection heat transfer of Al_2O_3–water nanofluid in a horizontal cylindrical enclosure with an inner triangular cylinder, Int. J. Heat Mass Transfer 80 (2015) 16–25.
[45] H.M. Elshehabey, S.E. Ahmed, MHD mixed convection in a lid-driven cavity filled by a nanofluid with sinusoidal temperature distribution on the both vertical walls using Buongiorno's nanofluid model, Int. J. Heat Mass Transfer 88 (2015) 181–202.
[46] M.A. Moussaoui, A. Mezrhab, H. Naji, A computation of flow and heat transfer past three heated cylinders in a vee shape by a double distribution MRT thermal lattice Boltzmann model, Int. J. Therm. Sci. 50 (2011) 1532–1542.
[47] M.E. McCracken, J. Abraham, Multiple-relaxation-time lattice-Boltzmann model for multiphase flow, Phys. Rev. E 71 (2005) 036701.
[48] Y. Qian, D. d'Humières, P. Lallemand, Lattice BGK models for Navier–Stokes equation, Europhys. Lett. 17 (1992) 479–484.
[49] P. Lallemand, L.-S. Luo, Theory of the lattice Boltzmann method: Dispersion, dissipation, isotropy, Galilean invariance, and stability, Phys. Rev. E 61 (2000) 6546–6574.
[50] Z. Guo, C. Zheng, B. Shi, T.-S. Zhao, Thermal lattice Boltzmann equation for low Mach number flows: decoupling model, Phys. Rev. E 75 (2007) 036704.
[51] A. Mezrhab, M.A. Moussaoui, M. Jami, H. Naji, M.h. Bouzidi, Double MRT thermal lattice Boltzmann method for simulating convective flows, Phys. Lett. A 374 (2010) 3499–3507.
[52] J. Wang, D. Wang, P. Lallemand, L.-S. Luo, Lattice Boltzmann simulations of thermal convective flows in two dimensions, Comput. Math. Appl. 65 (2013) 262–286.
[53] Q. Liu, Y.-L. He, Q. Li, W.-Q. Tao, A multiple-relaxation-time lattice Boltzmann model for convection heat transfer in porous media, Int. J. Heat Mass Transfer 73 (2014) 761–775.
[54] J.M. Garnett, Colours in metal glasses, in metallic films, and in metallic solutions. II, Philosophical Transactions of the Royal Society of London. Series A, Containing Papers of a Mathematical or Physical Character 205 (1906) 237–288.
[55] A. Akbarinia, A. Behzadmehr, Numerical study of laminar mixed convection of a nanofluid in horizontal curved tubes, Appl. Therm. Eng. 27 (2007) 1327–1337.
[56] E. Abu-Nada, Application of nanofluids for heat transfer enhancement of separated flows encountered in a backward facing step, Int. J. Heat Fluid Flow 29 (2008) 242–249.
[57] M. Rahman, S. Mojumder, S. Saha, A.H. Joarder, R. Saidur, A. Naim, Numerical and statistical analysis on unsteady magnetohydrodynamic convection in a semi-circular enclosure filled with ferrofluid, Int. J. Heat Mass Transfer 89 (2015) 1316–1330.
[58] H. Brinkman, The viscosity of concentrated suspensions and solutions, J. Chem. Phys. 20 (1952). 571-571.
[59] E. Abu-Nada, H.F. Oztop, Effects of inclination angle on natural convection in enclosures filled with Cu–water nanofluid, Int. J. Heat Fluid Flow 30 (2009) 669–678.
[60] N. Rudraiah, R. Barron, M. Venkatachalappa, C. Subbaraya, Effect of a magnetic field on free convection in a rectangular enclosure, Int. J. Eng. Sci. 33 (1995) 1075–1084.